Calculated spin polarization and magnetic dichroism of photoelectron diffraction spectra for magnetite below the Verwey temperature

P. Rennert,* W. Mück, and A. Chassé
Department of Physics, Martin-Luther-University Halle-Wittenberg, D-06099 Halle(Saale), Germany
(Received 5 December 1995)

Spin- and angular-resolved photoelectron spectra are calculated for magnetite below the Verwey temperature. The results are compared for the Mizoguchi model, the Zuo model, and an assumed nonmagnetic $Fe^{3+}Fe_2^{2.5+}O_4$ configuration. Due to an occurring symmetry breaking at the Verwey transition, the effect of the magnetization can be clearly separated from the spectra; further effects are due to charge ordering. Furthermore, the charge ordering models are compared by a separation of the spectra into contributions from ferrous and ferric ions. [S0163-1829(96)03321-8]

I. INTRODUCTION

Magnetite is a material which is investigated intensively, because it appears in rocks at depth, in biological objects, and because it is used for technical applications. It is responsible for palaeomagnetism and geomagnetic variations,[1] it can be important for the orientation of bees[2,3] and it is used in magnetic recording systems.[4,5]

Magnetite exhibits several structures. At the Verwey temperature $T_V \approx 119$ K there occurs a metal-insulator transition from a cubic to a monoclinic phase.[6,7] At very low temperatures we have arrangements due to magnetoelectric effects.[8,9] We find reconstructions at the surface[10,11] or in thin films.[12–14] A phase transition is found at high pressure.[15–17] Furthermore, Fe_3O_4/NiO multilayers[18–22] found considerable interest. The structure of these systems was investigated by neutron scattering,[23,24] low-energy electron diffraction,[14] photoelectron diffraction,[25,26] x-ray diffraction,[16,13] and other methods. There are attempts to determine the stable phase from electronic structure calculations.[27–31]

We discuss the possibilities to investigate the magnetic structure of Fe_3O_4 below the Verwey temperature using spin- and angular-resolved photoelectron diffraction. In Sec. II we resume the magnetic structure of different models. In Sec. III we summarize the basic formulas of the photoelectron diffraction. Calculated results are presented in Sec. IV and discussed in Sec. V. Section VI contains conclusions.

II. SYMMETRY CONSIDERATIONS

The first structure model for the monoclinic low-temperature phase was proposed by Verwey,[6] but was excluded by NMR measurements[32,33] and Mössbauer spectroscopy.[34,35] During the 1970s several models were proposed, which are reviewed in Ref. 7. At that time, the Mizoguchi model[32,36] seemed to be the most satisfactory one. However, it appeared to be slightly inconsistent with some neutron scattering experiments.[23] Overcoming this inconsistency Zuo et al.[27] proposed another model, which they confirmed by means of high-energy electron diffraction experiments. We want to investigate the possibility to decide by means of photoelectron diffraction experiments which of the two models of Mizoguchi and Zuo is more appropriate.

Therefore we compare both models with the fictive nonmagnetic high-temperature structure, regarding the charge ordering at the Verwey transition temperature and the magnetization as symmetry breakings.

At room temperature Fe_3O_4 has an inverse spinel structure, which is cubic with the lattice constant $a = 8.3963$ Å. The oxygen atoms nearly form a fcc lattice and the iron atoms occupy one-half and one-eighth of its octahedral (A) and tetrahedral (B) interstitial sites, respectively. The small deformation of the oxygen lattice[6] is not considered here. We find Fe^{3+} on the A sites and both Fe^{2+} and Fe^{3+} on the B sites; thus the inverse spinal structure can be characterized by the formula $Fe^{3+}(Fe^{2+}Fe^{3+})O_4$. However, as no distinction can be made between different B site atoms,[34,35,37] magnetite at room temperature is better described by $Fe^{3+}Fe_2^{2.5+}O_4$.

Magnetite is ferrimagnetic with the magnetic moments of the A and B site atoms showing opposite orientations. The magnetization has a cubic (111) direction at room temperature, whereas it changes to the monoclinic (001) direction for the low-temperature phase.[38]

Epitaxial growth of magnetite at room temperature leads to a [111] surface.[14] The stacking of layers for such a surface as determined by Barbieri et al.[14] is shown in Fig. 1. The positions of the iron atoms in each layer can be seen from Fig. 2. Focusing on the effects of the charge ordering we used the idealized inverse spinel positions also for the low-

FIG. 1. Layer stacking for a magnetite [111] surface without surface relaxation.
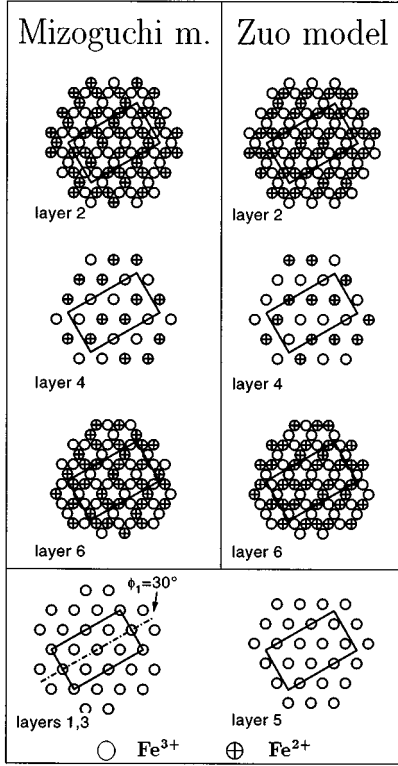
FIG. 2. Positions of the atoms in the iron layers of Fig. 1, counted from the surface downwards. Odd and even layers contain A and B site atoms, respectively. For room temperature all B site atoms must be thought to be $Fe^{2.5+}$. The two-dimensional unit cell of the monoclinic phase is shown in all layers.

temperature phase. The Mizoguchi and Zuo models differ from each other by the occupation of the B sites with Fe^{2+} and Fe^{3+} as shown in Fig. 2.

At room temperature the [111] surface configuration exhibits C_{3v} symmetry; i.e., there is a rotational C_3 symmetry around the surface normal and reflectional symmetries σ_i according to the three planes characterized by the polar angles[39] $\phi_1 = 30°(210°)$, $\phi_2 = 150°(330°)$, and $\phi_3 = 270°(90°)$. For both low-temperature models this symmetry is broken by charge ordering and the change of orientation of the magnetization, which is now described by the polar angles $\phi_m = 30°$ and $\theta_m \approx 54.7°$. While the Mizoguchi model shows no symmetries for the [111] surface, there remains a glide plane for $\phi_1 = 30°$ (see Fig. 2) in the Zuo model, which, in view of the direction of the magnetization, favors this model. The consequences of the symmetry breakings for the photoelectron spectra are discussed in the next section.

III. THEORY

We calculate the photoelectron current dependent on the direction (photoelectron wave vector $\mathbf{k}$), the photoelectron spin (quantum number σ), and the photon polarization $\vec{\epsilon}$. The arbitrary polarization

$$\vec{\epsilon} = \mathbf{e}_1 \sin\alpha + \mathbf{e}_2 e^{i\xi}\cos\alpha \qquad (1)$$

can be described by two angles α and ξ. $\mathbf{e}_{1,2}$ are unit vectors perpendicular to the photon wave vector; $\mathbf{e}_2$ is chosen to be parallel to the surface. For $\alpha = \pi/4$ and $\xi = \pm \pi/2$ we have right and left circularly polarized light, depending, respectively, on the sign of ξ.

The photoelectron intensity

$$I_c^\sigma(\mathbf{k}) \sim \sum_{\mathbf{R}} \sum_{\mu_c} \left| \sum_L B_{RL}^\sigma(\mathbf{k}) M_{L\sigma,c} \right|^2 \qquad (2)$$

is a sum over the contributions of the degenerated core levels μ_c at different sites $\mathbf{R}$. For our notation we refer to Refs. 40 and 26. M is the dipole matrix element and B the scattering path operator, which contains the direct wave and the single and multiple scattering contributions. Generally, the scattering phase shifts δ_l depend on the spin σ.

We consider the transformation of the intensity (2) with respect to the rotation C_3 and the reflections σ_i ($i = 1,2,3$) assuming that these symmetries are present and the (111) direction is the axis of spin quantization. We restrict the formulas on a photon wave vector parallel (or antiparallel) to the (111) direction and right ($\vec{\epsilon}$, rc) or left ($\vec{\epsilon}^*$, lc) circularly polarized light. The direction of the photoelectron wave vector $\mathbf{k}$ is described by the two polar angles θ and ϕ.

Applying C_3 leaves the spinors and the photon polarization invariant. Therefore we find for the spin-dependent intensities

$$I^\sigma(\theta,\phi;\vec{\epsilon}) = I^\sigma(\theta,120° + \phi;\vec{\epsilon}). \qquad (3)$$

The reflections σ_i change the spinor from spin up to spin down and vice versa (as shown in the Appendix) and the polarization from $\vec{\epsilon}$ to $\vec{\epsilon}^*$. If the scattering potential is not spin dependent, we find the relation

$$I^\sigma(\theta,\phi_i + \phi;\vec{\epsilon}) = I^{-\sigma}(\theta,\phi_i - \phi;\vec{\epsilon}^*). \qquad (4)$$

Obviously both Eqs. (3) and (4) apply also for the total intensity.

From (3) and (4) symmetry relations for the dichroism, $D = (I_{rc}^\uparrow + I_{rc}^\downarrow) - (I_{lc}^\uparrow + I_{lc}^\downarrow)$, and for the spin polarization, $P(\vec{\epsilon}) = \{I^\uparrow(\vec{\epsilon}) - I^\downarrow(\vec{\epsilon})\}/\{I^\uparrow(\vec{\epsilon}) + I^\downarrow(\vec{\epsilon})\}$, can be derived, giving

$$D(\theta,\phi) = D(\theta,120° + \phi), \qquad (5)$$

$$P(\theta,\phi,\vec{\epsilon}) = P(\theta,120° + \phi,\vec{\epsilon}) \qquad (6)$$

and

$$D(\theta,\phi_i + \phi) = -D(\theta,\phi_i - \phi), \qquad (7)$$

$$P(\theta,\phi_i + \phi,\vec{\epsilon}) = -P(\theta,\phi_i - \phi,\vec{\epsilon}^*). \qquad (8)$$

In magnetite we find a breaking of the symmetry relations (3) and (4) due to the lattice distortion, the magnetization, and the charge ordering below the Verwey temperature. We only discuss the influence of the magnetization and the charge ordering. Still above the Verwey temperature there occurs a breaking of (4), if we include the spin dependence of the scattering potential. This effect gives rise to the possibility to study the magnetic structure of magnetite above
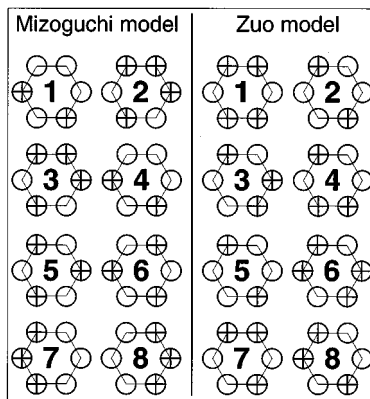
FIG. 3. The eight different rings of layer 2 for the Mizoguchi and Zuo models.

the Verwey temperature and was investigated in an earlier paper.[26] Below the Verwey temperature both relations (3) and (4) are broken. In addition, the axis of spin quantization, which coincides with the direction of the magnetization, is now different from the surface normal. Therefore Eq. (3) would not hold for the spin-dependent intensities, even if the crystal symmetry still contained C_3. However, it would still hold for the total intensity, because the choice of the axis of spin quantization does not affect the scalar total intensity. Accordingly (5) would still hold. On the other hand, Eqs. (4), (7), and (8) still hold in the spin-independent case, but due to the direction of the magnetization only for $\phi_1 = \phi_m = 30°$.

We calculate the strength of the breaking of these symmetries and its difference for the charge ordering models of Mizoguchi and Zuo.

IV. CALCULATIONS

Within the multiple scattering theory the atoms are characterized by scattering phase shifts. In our system they are different for Fe^{2+} and Fe^{3+} due to the different atomic configurations $3d^5$ and $3d^4$, respectively. Furthermore, at each site we have different phase shifts for spin up and spin down electrons, because the exchange potential is determined by the number of electrons with parallel spin. Details of these considerations can be found in Ref. 26.

Above the Verwey temperature the electron configurations $3d^4 4s^1$ and $3d^{4.5} 4s^1$ were used to describe Fe^{3+} on the A sublattice and $Fe^{2.5+}$ on the B sublattice, respectively. The spin is quantized along the (111) axis, which is the surface normal for epitaxial-grown magnetite. Below the Verwey temperature we have a change of the magnetization direction from (111) to (001). Moreover, in the B sublattice we have a definite distribution of Fe^{2+} and Fe^{3+}, which is different for the Mizoguchi and Zuo models.

As can be seen in Fig. 2, there are eight nonequivalent atoms in the 2D unit cell of layer 1. Lying just underneath in layer 2 there are eight rings of six atoms, each atom being contained in two rings. The eight rings of layer 2 are shown in Fig. 3 for the Mizoguchi and Zuo models. The distribution of Fe^{2+} and Fe^{3+} atoms within the rings differs between the two models. Thus, the difference in the contribution of these rings to the photoelectron spectra determines the order of magnitude of the difference in the spectra between the Zuo
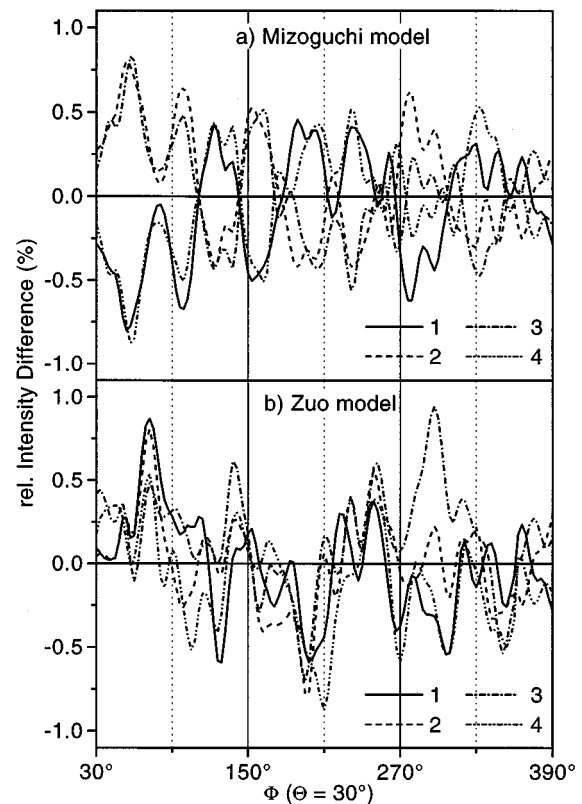

FIG. 4. Calculated relative differences of the total intensities between rings 1–4 of the Mizoguchi (a) and Zuo (b) models and the hypothetical unordered structure, both nonmagnetic. The normalized entity $(I_{ring} - I_{unord})/(2I_{unord})$ is shown.

model, the Mizoguchi model, and the hypothetical $Fe^{3+}Fe_2^{2.5+}O_4$, i.e., the idealized high-temperature configuration.

We calculated the photoelectron spectra for the different rings 1–8 (see Fig. 3) within the Mizoguchi and Zuo models, and we compare the results with the nonmagnetic high-temperature configuration in Fig. 4. The same lattice constant was used for all calculations. The differences characterize the order of magnitude of the magnetic scattering, which is different for the different structure models.

Another possibility to distinguish between the Mizoguchi and Zuo models is to separate the spectra of Fe^{2+} and Fe^{3+}. Sasaki[41] observed a chemical shift of about 5 eV between the ferrous and ferric ions in x-ray absorption near-edge structure (XANES) measurements. Therefore we calculated the contributions from Fe^{2+} and Fe^{3+} to the photoelectron spectra separately as shown in Fig. 5. The different total intensities for the Fe^{2+} and Fe^{3+} atoms [Fig. 5(a)] stem from the different total number of absorbers. The intensity for Fe^{3+} is roughly twice the intensity for Fe^{2+}.

All calculations were performed for an electron energy of 70 eV and up to the first scattering order, which is sufficient to estimate the order of magnitude of the influence of the magnetic scattering. The excited core state was taken to be the $p_{1/2}$ state, which differs energetically by approximately 13 eV from the $p_{3/2}$ state.[42] Therefore, both states can be clearly separated in experiments. The calculations were performed for a cluster of 174 iron atoms with a (111) surface. The oxygen atoms were neglected for these qualitative con-
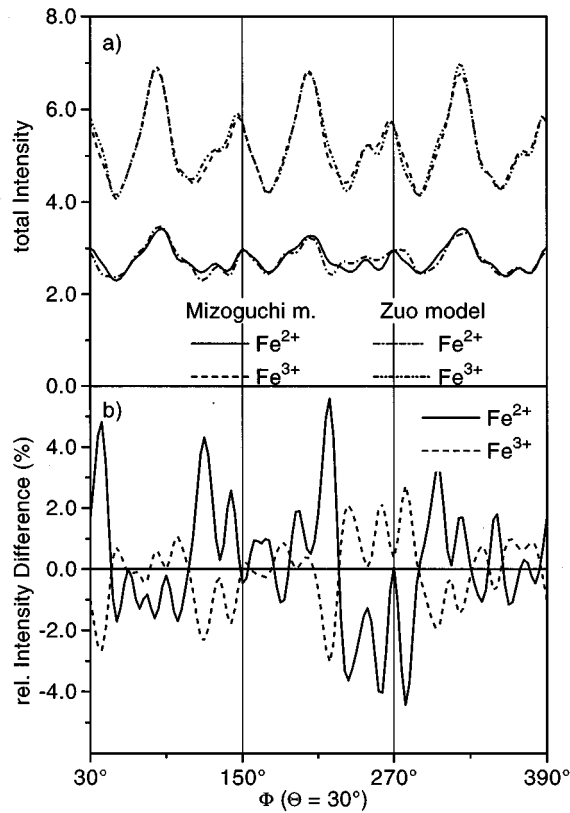
FIG. 5. Calculated total intensities for the Mizoguchi and Zuo models with the contributions of the Fe^{2+} and Fe^{3+} absorbers shown separately (a). The relative intensity difference (b) between both models is given by $(I_{Miz}-I_{Zuo})/(I_{Miz}+I_{Zuo})$.
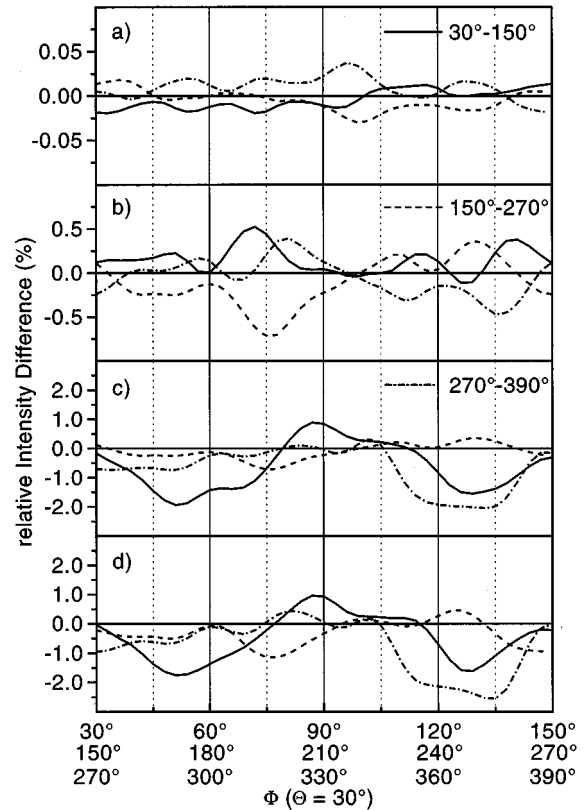

FIG. 6. Calculated relative differences (cf. Fig. 4) between the total intensities for the Mizoguchi (a), (b) and Zuo (c), (d) models and the total intensity for the hypothetical nonmagnetic unordered structure. For (a) and (c) the magnetic moment was not included, whereas it was included for (b) and (d). The three intervals of the polar angle ϕ are compared in order to illustrate the C_3 symmetry breaking. Note the different axis scales.

siderations, as they are weak scatterers. The direction of the incident photons was taken to be perpendicular to the (111) surface. The electron spin was quantized parallel to the magnetic moment, i.e., in the (001) direction.

V. DISCUSSION

Besides the lattice distortion we have two sources for the symmetry breaking. (i) The charge ordering at the B sites is represented by the fact that Fe^{2+} and Fe^{3+} are assigned different atomic potentials due to their different electron configurations. The atomic distribution shows neither the C_3 nor the σ_i symmetry (see Fig. 2). Only in the Zuo model does there remain a glide symmetry. (ii) Due to the magnetic moment of the atoms, the exchange potential is different for spin up and spin down electrons, which results in their different scattering properties. This leads to an additional breaking of the σ_1 symmetry.

Figure 4 shows the contributions of rings 1–4 (see Fig. 3) to the photoelectron diffraction spectra, including (i), but neglecting (ii) at first. Due to the different numbers and positions of the Fe^{2+} and Fe^{3+}, we find a violation of C_3 [formula (3)] of about 1% compared with the hypothetical $Fe^{3+}Fe_2^{2.5+}O_4$ configuration. However, if we add up all the contributions, then there nearly occurs a cancellation in the Mizoguchi model [Fig. 6(a)], whereas more than 10 times larger differences remain in the Zuo model [Fig. 6(b)]. The reason is the relatively arbitrary distribution of the Fe^{2+} and Fe^{3+} atoms in the Mizoguchi model. In the eight rings of

layer 2 (see Fig. 3) each position is occupied 4 times by Fe^{2+} and 4 times by Fe^{3+}. Moreover, the contributions of rings 1 and 2 as well as of rings 3 and 4 to the symmetry breaking nearly cancel, as can be seen in Fig. 4; the same is true for rings 5–8. On the other hand, for the Zuo model the atoms form three-atom chains in certain directions (see Fig. 2). Thus, the upper left and lower right positions of the rings are always occupied by Fe^{2+}. Therefore the contributions of the single rings to the symmetry breaking do not cancel. If the magnetic scattering (ii) is included, then the symmetry breaking is observable also in the Michoguzi model [Fig. 6(c)] and is enhanced in the Zuo model [Fig. 6(d)]. Hence, the overall C_3 symmetry breaking is mainly determined by the fact that the magnetization is not orientated along (111). In addition, the charge ordering results in differences between the spectra for the Mizoguchi and Zuo models.

Figure 7 shows the relative symmetry breaking of Eq. (4). Neglecting the magnetic scattering (ii) there is nothing but a small symmetry breaking for the Mizoguchi model as well as for the Zuo model [Fig. 7(a)]. For the Mizoguchi model this derives from a cancellation similar to the results shown in Fig. 6(a); for the Zuo model it follows from the existing glide symmetry. Including the magnetic scattering [Fig. 7(b)] a symmetry breaking of some percent arises. As can be seen, the overall σ_1 symmetry breaking nearly exclusively stems from the magnetization, which is the same for both structure
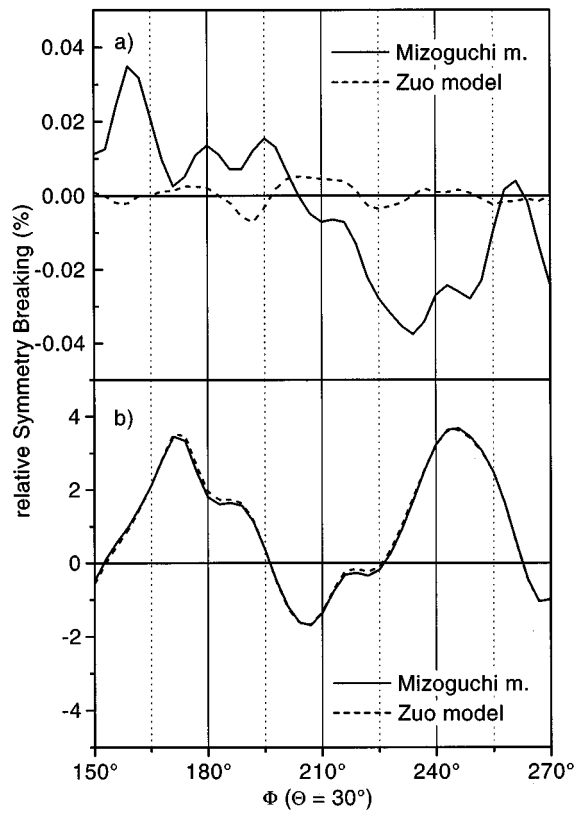
FIG. 7. Calculated σ_1 symmetry breaking for the Mizoguchi and Zuo models. The relative entity $[I_{rc,\uparrow}(210°+\phi)-I_{lc,\downarrow}(210°-\phi)]/[I_{rc,\uparrow}(210°+\phi)+I_{lc,\downarrow}(210°-\phi)]$ is shown. For (a) the magnetic moment was not included; for (b) it was. Note the different axis scales.

models. Therefore, for these results the difference between the Mizoguchi and Zuo models is very small.

VI. CONCLUSIONS

The aim of this paper was to consider different possibilities to investigate the charge ordering of magnetite below the Verwey transition temperature by means of spin- and angular-resolved photoelectron diffraction experiments, particularly if one can distinguish between the Mizoguchi and Zuo models. Using the occurring symmetry breaking of measured spectra is a suitable tool, because interesting effects can be separated from the spectra and only a little quantitative comparison with model calculations is needed. Two different possibilities of this investigation have been found. First, of the two symmetry breakings C_3 and σ_1 only the

former shows measurably different spectra for the Mizoguchi and Zuo models and can therefore be used to investigate charge ordering, whereas the latter is dominated by the magnetic symmetry breaking and contains too small an amount of information about charge ordering. Because only the total intensities are needed for the C_3 symmetry breaking, simple, i.e., not spin-polarized, photoelectron diffraction experiments are sufficient for this particular investigation. Second, if the spectra for the ferrous and ferric ions are considered separately, the spectra are measurably different for both charge ordering models. Moreover, the C_3 symmetry breaking turns out even clearer. Hence, a combination of both methods yields an excellent possibility to study the charge ordering of magnetite below the Verwey temperature.

APPENDIX

Without loss of generality, we consider the transformation of a spinor with respect to a reflexion at the yz plane. The transformation $(x,y,z)\rightarrow(-x,y,z)$ may be split up into a 180° rotation around the x axis $(x,y,z)\rightarrow(x,-y,-z)$ and the inversion $(x,-y,-z)\rightarrow(-x,y,z)$. The transformation of a four-component spinor by the inversion is given by a multiplication with the Dirac matrix $-i\gamma_4$.[43] If we restrict our considerations to two-component spinors, the spinor is not changed, because there is no two-dimensional irreducible unitary representation of improper rotations.

The change of any physical quantity by a rotation $\delta\boldsymbol{\omega}$ is given by the unitary transformation matrix $U=\exp[-(i/\hbar)\boldsymbol{J}\cdot\delta\boldsymbol{\omega}]$. For a finite rotation $\boldsymbol{\omega}$ around a certain axis, $\delta\boldsymbol{\omega}$ can be replaced by $\boldsymbol{\omega}$. If we restrict our considerations to the transformation of the two-component spinors, $\boldsymbol{J}$ coincides with the spin operator $(\hbar/2)\boldsymbol{\sigma}$, where $\boldsymbol{\sigma}$ is the vector of the Pauli matrices. For $\boldsymbol{\omega}=\omega\boldsymbol{e}_x$ we find

$$U=I\cos(\omega/2)-i\sigma_x\sin(\omega/2),$$

which simplifies because of $\sigma_x^2=I$. In this particular case, $\omega=\pi$; thus only $U=-i\sigma_x$ remains. With

$$\sigma_x=\begin{pmatrix} 0 & 1 \\ 1 & 0 \end{pmatrix}, \quad \chi_+=\begin{pmatrix} 1 \\ 0 \end{pmatrix}, \quad \chi_-=\begin{pmatrix} 0 \\ 1 \end{pmatrix}$$

we obtain

$$U\chi_+=-i\chi_- \quad \text{and} \quad U\chi_-=-i\chi_+.$$

Thus, up to a phase factor, which does not contribute to any matrix element, the spin up and spin down spinors are exchanged. Equation (4) follows from this result.

*Electronic address: rennert@physik.uni-halle.d400.de

[1] J.W. Holt and J.L. Kirschvink, Earth and Planetary Sci. Lett. **133**, 475 (1995).

[2] H. Schiff and G. Canal, Biol. Cybern. **69**, 7 (1993).

[3] J.L. Kirschvink, A. Kobayashi-Kirschvink, J.C. Diaz-Ricci, and S.J. Kirschvink, Bioelectromagnetics **1**, 101 (1992).

[4] F.T. Parker, F.E. Spada, T.J. Cox, and A.E. Berkowtiz, J. Appl. Phys. **77**, 5853 (1995).

[5] C.H. Lin, P.C. Kuo, J.A. Chen, and Y.D. Yao, IEEE Trans. Magn. **MAG-30**, 4104 (1994).

[6] E.J.W. Verwey and P.W. Haayman, Physica **8**, 979 (1941).

[7] N.F. Mott *et al.*, Philos. Mag. **42**, 327-432 (1980).

[8] Y. Miyamoyto, Ferroelectrics **161**, 117 (1994).

[9] Y. Miyamoto, S. Ishihara, T. Hirano, M. Takada, and N. Suzuki, Solid State Commun. **89**, 51 (1994).

[10] R. Jansen, B.J. Nelissen, D.L. Abraham, H. van Kempen, and V.A.M. Brabers, IEEE Trans. Magn. **MAG-30**, 4506 (1994).

[11] G. Tarrasch, D. Burgler, T. Schaub, R. Wesendanger, and N.J. Guntherodt, Surf. Sci. **285**, 1 (1993).

[12] C.A. Kleint, H.C. Semmelhack, M. Lorenz, and M.K. Krause, J.

Magn. Magn. Mater. **140-144**, 725 (1995).

[13] H.C. Choi, J.S. Ahn, W. Jo, T.W. Noh, S.H. Chun, and Z.G. Khim, in *Epitaxial Oxide Thin Films and Heterostructures,* edited by D. K. Fork, J. M. Phillips, R. Ramesh, and R. M. Wolf, MRS Symposia Proceedings No. 341 (Materials Research Society, Pittsburgh, 1995), p. 35.

[14] A. Barbieri, W. Weiss, M.A. Van Hove, and G.A. Somorjai, Surf. Sci. **302**, 259 (1994).

[15] P.R. Kelso and S.K. Banerjee, Geophys. Res. Lett. **22**, 1953 (1995).

[16] L. Gerward and J.S. Olsen, Appl. Radiat. Isot. **46**, 553 (1995).

[17] M.P. Pasternak, S. Nasu, K. Wada, and S. Endo, Phys. Rev. B **50**, 6446 (1994).

[18] D.M. Lind, J.A. Borchers, R.W. Erwin, J.F. Anker, E. Lochner, K.A. Shaw, R.C. Di Bari, W. Portwine, P. Stoyonov, and S.D. Berry, J. Appl. Phys. **76**, 6284 (1994).

[19] S.D. Berry, D.M. Lind, G. Chern, and H. Mathias, J. Magn. Magn. Mater. **123**, 126 (1993).

[20] J.J. Krebs, D.M. Lind, E. Lochner, K.A. Shaw, W. Portwine, and S.D. Berry, J. Appl. Phys. **75**, 6688 (1994).

[21] J.A. Borchers, R.W. Erwin, J.F. Ankner, S.D. Berry, D.M. Lind, E. Lochner, and K.A. Shaw, J. Appl. Phys. **75**, 6692 (1994).

[22] S.D. Berry, J.A. Borchers, R.W. Erwin, D.M. Lind, K.A. Shaw, and E. Lochner, J. Appl. Phys. **75**, 6691 (1994).

[23] M. Iizumi, T.F. Koetzle, G. Shirane, S. Chikazumi, M. Matsui, and S. Todo, Acta Crystallogr. B **38**, 2121 (1982).

[24] M. Iizumi and G. Shirane, Solid State Commun. **17**, 433 (1975).

[25] Y.J. Kim, C. Westphal, R.X. Ynzunza, H. Xiao, Z. Wang, H.C. Galloway, M. Salmeron, M.A. Van Hove, and C.S. Fadley, J. Electron Spectrosc. (to be published).

[26] P. Rennert, W. Mück, and A. Chassé, Surf. Sci. (to be published).

[27] J.M. Zuo, J.C.H. Spence, and W. Petuskey, Phys. Rev. B **42**, 8451 (1990).

[28] M. Uhl and B. Siberchicot, J. Phys. **7**, 4227 (1995).

[29] S.K. Mishra and S. Satpathy, Phys. Rev. B **47**, 5564 (1993).

[30] M. Samiullah, Phys. Rev. B **51**, 10352 (1995).

[31] S.K. Mishra, Z. Zhang, and S. Sathpathy, J. Appl. Phys. **76**, 6700 (1994).

[32] M. Mizoguchi, J. Phys. Soc. Jpn. **44**, 1501 (1978); **44**, 1512 (1978).

[33] U. Buchenau, Phys. Status Solidi A **29**, K47 (1975).

[34] B.J. Evans and S.S. Hafner, J. Appl. Phys. **40**, 1412 (1969).

[35] H. Weber and S.S. Hafner, Z. Kristallogr. **133**, 331 (1971).

[36] S. Iida, Philos. Mag. **42**, 349 (1980).

[37] A. Yanase and K. Siratori, J. Phys. Soc. Jpn. **53**, 312 (1984).

[38] If not indicated otherwise, we use cubic indexing for the notation of lattice and reciprocal vectors. However, the cubic and the monoclinic (001) directions coincide.

[39] The polar coordinate system is introduced such that $\theta=0$ describes the [111] surface normal and $\theta=90°, \phi=0$ represent a horizontal line in Fig. 2, orientated to the right.

[40] P. Rennert and A. Chassé, Exp. Tech. Phys. **35**, 27 (1987).

[41] S. Sasaki, Rev. Sci. Instrum. **66**, 1573 (1995).

[42] D.A. Shirley, R.L. Martin, S.P. Kowalczyk, F.R. Feely, and L. Ley, Phys. Rev. B **15**, 544 (1977).

[43] J.F. Cornwell, *Group Theory in Physics* (Academic Press, London, 1984), Vol. 2, p. 699.